ACS OMEGA

Article

Cite This: ACS Omega 2019, 4, 13034−13041

http://pubs.acs.org/journal/acsodf

Charged Nanoparticles Quench the Propulsion of Active Janus Colloids

Marola W. Issa,[†,§] Nicky R. Baumgartner,[‡,§] Mohammed A. Kalil,[†] Shawn D. Ryan,[‡] and Christopher L. Wirth*[,†]

[†]Department of Chemical and Biomedical Engineering, Washkewicz College of Engineering and [‡]Department of Mathematics and Statistics, College of Science and Health Professions, Cleveland State University, 2121 Euclid Avenue, Cleveland, Ohio 44115, United States

ABSTRACT: Active colloidal particles regularly interact with surfaces in applications ranging from microfluidics to sensing. Recent work has revealed the complex nature of these surface interactions for active particles. Herein, we summarize experiments and simulations that show the impact of charged nanoparticles on the propulsion of an active colloid near a boundary. Adding charged nanoparticles not only decreased the average separation distance of a passive colloid because of depletion attraction as expected but also decreased the apparent propulsion of a Janus colloid to near zero. Complementary agent-based simulations considering the impact of hydrodynamics for active Janus colloids were conducted in the range of separation distances inferred from experiment. These simulations showed that propulsion speed decreased monotonically with decreasing average separation distance. Although the trend found in experiments and simulations was in qualitative agreement, there was still a significant difference in the magnitude of speed reduction. The quantitative difference was attributed to the influence of charged nanoparticles on the conductivity of the active particle suspension. Follow-up experiments delineating the impact of depletion and conductivity showed that both contribute to the reduction of speed for an active Janus particle. The experimental and simulated data suggests that it is necessary to consider the synergistic effects between various mechanisms influencing interactions experienced by an active particle near a boundary.

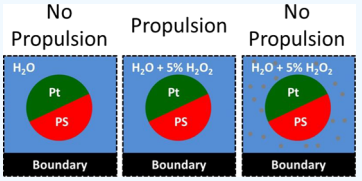

1. INTRODUCTION

Micrometer-scale self-propelled or active "colloidal" particles that generate force to induce motion have the potential as microscale cargo carriers, chemical sensors, and synthetic analogs for micro- and macroscale biological entities.[1−7] Active colloids generate sufficient force for motility through a combination of a local break in symmetry and an environmental cue that actuates motion.[8,9] Propulsion can be generated by a chemical reaction, light, magnetic, and electric fields.[10−13] One such example is that of a patchy sphere comprising a native particle with a metallic cap.[14] The patchy sphere is called a "Janus" particle when the cap covers approximately ∼50% of the available surface area. Janus particle caps typically have a nominal thickness of 5−30 nm that will vary across the contour of the particle as a consequence of the fabrication process,[15] which can also be adjusted to tune the cap size and shape.[16−18] Janus particles consisting of an arbitrary native particle and a platinum cap propel in the presence of hydrogen peroxide (H_2O_2) because of a decomposition reaction on the platinum cap. Reactants and products form a gradient in solute on the length scale of the particle that induces self-diffusiophoretic motion.[19] Propulsion speed increases with fuel concentration, ranging from ∼0.1 to 10 μm/s. Graphite-capped particles are the second example of a Janus particle that propels in response to a cue.[10] Local demixing of the solvent in the vicinity of the graphite cap occurs when the particle is heated via illumination by a focused light source at the wavelength of absorption for graphite around 532 nm. The latter system has the advantage of being reversible, yet requires an external source of actuation. Given that active Janus particles move as a consequence of "self-generated" motion, these synthetic systems offer an intriguing option for studying phenomena typically found in biology, for instance, swarming, clustering, or interaction with nearby surfaces.

Just like "passive" colloids, active colloids regularly interact with surfaces,[20] via both conservative (i.e., path-independent) and nonconservative (i.e., path-dependent) interactions. Conservative interactions typically arise from physiochemical properties of the fluid, whereas nonconservative interactions are hydrodynamic in nature. Conservative surface interactions may depend on system properties such as the salinity, particle charge, or number concentration of dispersed solids. Nonconservative interactions typically depend on the inherent geometry of the system, such as particle confinement or shape. The combination of these forces is known to play a critical role in the dynamics of passive particles near boundaries, especially when multiple particles are being considered.[21] More recently, surface interactions have been elucidated for active particles near boundaries, where additional consideration such as that of disturbances to local fuel concentration by the nearby boundary was considered.[20,22−26] One recent example showed

Received: March 19, 2019
Accepted: July 25, 2019
Published: August 9, 2019

that the rotational diffusion of a platinum-capped Janus particle was quenched near a boundary, subsequently steering the propulsion of the particle along a corner because of hydrodynamic quenching.[27] This work highlights a hydrodynamic strategy for steering active colloids, which will be necessary to realize the full potential of active systems for applications.

This paper summarizes experiments and simulations of an active particle near a boundary. Micrometer-scale Janus particles with platinum caps in the presence of H_2O_2 were imaged and tracked, and the apparent propulsion speed was calculated from the mean-squared displacement (MSD) in the presence and absence of negatively charged nanoparticles. Nominally, 5 μm diameter Janus particles near a boundary propelled at speeds from 0.1 to 2 μm/s in response to H_2O_2 but had a propulsion speed approaching 0 μm/s following the addition of strongly charged 20 nm particles. A separate set of experiments found that the average apparent separation distance of passive colloidal particles in the absence of H_2O_2, but in the presence of nanoparticles, was reduced to <100 nm. Quasi-two-dimensional (2D) agent-based simulations were conducted to infer the change in propulsion speed from hydrodynamics in response to this apparent change in separation distance. Simulations showed that the speed was reduced as a consequence of a change in separation distance, but the magnitude of the reduction was insufficient to account for experimental observations. Further measurements showed that the conductivity of the suspensions increased upon the addition of the nanoparticle depletants. Increasing the conductivity of the fluid has been shown to decrease the propulsion speed of active particles under the influence of self-electrophoresis.[28] Follow-up measurements controlling for the influence of charge in a depletant system showed that both fluid conductivity and depletion attraction were relevant to slowing the propulsion speed of active Janus particles. Observations from simulations and experiments summarized herein demonstrate the importance of considering both conservative and nonconservative surface interactions experienced by an active colloid near a boundary, in addition to any fluid constituents that may impact the propulsion mechanism.

2. THEORY

2.1. Dynamics of a Janus Particle Near a Boundary.

Consider a single spherical particle as shown in Figure 1. The particle has radius a and is separated a distance h from the nearby boundary. The particle experiences random fluctuations in both position (x, y, z) and orientation (θ, ϕ) because of collisions between it and neighboring solvent molecules (i.e., Brownian motion). The particle is sampling positions in a potential energy well comprising conservative forces that are a consequence of the chemistry or topology of the particle and surface. The particle remains mobile because of the strong electrostatic repulsion between it and the neighboring boundary. In addition to conservative interactions, the particle experiences nonconservative hydrodynamic forces and torques in response to both translational and rotational motion, respectively.[29] The work described herein is primarily concerned with motion in the xy-plane. The drag in response to the translational motion in the xy-plane is the wall-corrected Stokes drag force

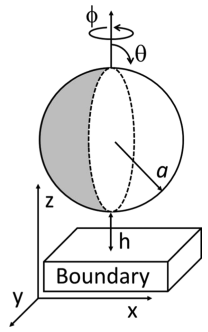

Figure 1. Janus particle with radius a and separation distance h. A micrometer-scale Janus particle with a density not matching that of the solvent will settle to the bottom boundary of a fluid cell. The particle will experience Brownian fluctuations in position (x, y, z). Experiments and simulations described herein track and infer speed from motion in the xy-plane. Once near the boundary, the particle will have an instantaneous separation distance h that is characterized with a most probable h_m or average separation distance h_{AVG}. Upon the addition of hydrogen peroxide (H_2O_2) to a solution, the particle will move along a deterministic path in the xy-plane.

$$\mathbf{F_d} = \frac{f_\infty}{q^{xy}(\delta)}\frac{d\mathbf{x}}{dt} = \frac{6\pi\eta a}{q^{xy}(\delta)}\frac{d\mathbf{x}}{dt} \quad (1)$$

$$q^{xy}(\delta) = \frac{12420\delta^2 + 5654\delta + 100}{12420\delta^2 + 12233\delta + 431} \quad (2)$$

where f_∞ is the linear quasi-steady Stokes drag coefficient, η is the fluid viscosity, $q^{xy}(\delta)$ is the wall correction factor in the xy-plane, $\mathbf{x}$ is the position vector, and $\delta = h/a$. Similarly, the drag in response to rotational motion in the relevant rotational axis is

$$\mathbf{T_d} = \frac{f^r_\infty}{q^\theta(\delta)}\frac{d\omega}{dt} = \frac{8\pi\eta a^3}{q^\theta(\delta)}\frac{d\omega}{dt} \quad (3)$$

$$q^\theta(\delta) = \left(1 + \frac{5}{16}\left(\frac{1}{\delta + 1}\right)^3\right)^{-1} \quad (4)$$

where $f_\infty{}^r$ is the rotational drag coefficient for a particle far from the boundary, $d\omega/dt$ is the rotational rate, and $q^\theta(\delta)$ is the wall correction factor for θ rotation. Equations 1−4 are for the quasi-steady translation or rotation of a sphere near a boundary. These expressions are appropriate when both the Reynolds $(va\rho_f/\eta)$ and the product of the Stokes numbers $(a^2\rho_f/T\eta)$ are small, where T is the characteristic time scale of the flow. Considering the small size of a typical particle (~1−10 μm) and the self-propelled velocity typically encountered in experiments (~0.1−5 μm/s), both of these dimensionless numbers are small. These quantities are similar to those of a swimming bacterium such as *Escherichia coli*, which has been successfully studied with models in the low Reynolds number regime by the present authors among others.[30−32] The main advantage to this approach is that in place of the nonlinear Navier−Stokes equations one can model the fluid and interaction with surrounding particles using a linear Stokes equation.

2.2. Agent-Based Modeling. We developed a differential-equation-based model derived from the balance of forces and torques on each platinum-capped particle. The key feature is that the model represents each Janus particle as a point force dipole. While the Janus particles themselves are propelled by a

DOI: 10.1021/acsomega.9b00765
ACS Omega 2019, 4, 13034−13041

chemical reaction, the net result of motion is the same as a self-propelled particle such as a swimming bacterium beating its flagella to propel through the fluid. Here, the Janus cells are spheres, whereas typically bacteria are elliptical in shape quantified by the Bretherton constant ($B = 0/1$ for sphere/needles). However, the propulsion mechanism for any shape can be modeled as a point force dipole where the drag force on the body is balanced by the propulsion force. The shape plays a greater role in the dynamics of the orientation of a cell than in the translational velocity.

The point dipole model tracks the motion of a particle's center of mass and orientation, which are both crucial for understanding the dynamics at the microscale. Extensive work using models of this form has successfully captured the experimental observation for isolated and collective bacterial motion.[30,33−36] In particular, the streamlines generated by the model are qualitatively the same as the recent experimental observation everywhere but within a half-particle length of the cell.[37] This discrepancy only becomes relevant at high concentrations or locally dense regions of active particles. To account for this, an excluded volume force is implemented modeling soft collisions at the microscale. A distinct advantage of using this form is the simple nature of the numerical simulations that allow for tracking many particles in a modest amount of computational time. The efficiency comes from an explicit analytical solution to the fluid equation describing the hydrodynamic velocity field generated by each Janus particle.

In particular, we consider N point particles representing the Janus cells indexed from $i = 1, ...,N$. The model will account for the dynamics of the center of mass $\mathbf{x}_i \in \mathbb{R}^2$ and orientation $\mathbf{d}_i \in \mathcal{S}^1$, a unit vector. Given the typical movement speed of the Janus particles (∼0.1−5 μm/s) and the typical size (2.5−5 μm), the fluid is in the low Reynolds number regime. This allows the fluid to be modeled as a linear Stokes equation avoiding the complexity of solving the full Navier−Stokes equations. As in the experimental setup, we consider a thin-film model where the length component in the z-direction is much less than in the xy-directions tangent to the bottom surface. Previous work derived an explicit analytical solution for the point dipole flow in a thin film, which is taken as the limit of two oppositely oriented force monopoles.[31,38] The primary difference between the thin-film fluid velocity and the free space is the decay rate as a function of separation distance. The former decays as the inverse cube of the distance, while the latter decays as the inverse square.

We assume for the model that the particles are all at the same height away from the boundary h, allowing for the treatment of the system as if it were quasi-2D. Therefore, the expression used for the fluid velocity at $\mathbf{x}\in\mathbb{R}^2$ time t generated by a Janus particle at the origin with orientation $\mathbf{d}_i$ is given by

$$\mathbf{u}(\mathbf{x}, t) = -\frac{U_0(a+h)}{3\pi}\sum_{i=1}^{N}\{\nabla^3[\log(|\mathbf{x}-\mathbf{x}_i(t)|)]\cdot\mathbf{d}_i(t)\}\mathbf{d}_i(t) \tag{5}$$

where $U_0 = \zeta\eta l^2 v_0 > 0$ is the size of the cell dipole moment derived from the Stokes drag law, where ζ is a shape coefficient, which is 6π for spheres using the classic Stokes drag law, η is the ambient fluid viscosity, v_0 is the isolated movement speed of a Janus particle, and l is the particle diameter.[31] Also, $a + h$ is the height of the center of mass above the bottom surface. The sum is a result of being in a semidilute regime where the total N body hydrodynamic interactions on a given particle are the sum of pairwise flows generated by each other active particle on that particle's location in the domain. Since this is a low Reynolds number fluid, the dynamics will be overdamped resulting in the velocity being proportional to force (e.g., Stokes drag law). Thus, from the balance of forces and torques on each Janus particle, we have

$$\dot{\mathbf{x}}_i = q_{xy}\left(v_0\mathbf{d}_i + \mathbf{u}(\mathbf{x}_i, t) + \frac{1}{6\pi\eta a}\sum_{i\neq j}^{N}\mathbf{F}(\mathbf{x}_i - \mathbf{x}_j) + \sqrt{D_t}\frac{dW}{dt}\right) \tag{6}$$

$$\dot{\mathbf{d}}_i = q_\theta\left(-\mathbf{d}_i\times[\nabla\times\mathbf{u}] + \sqrt{D_\theta}\frac{dW}{dt}\right) \tag{7}$$

The first term in the translational velocity equation represents the self-propulsion of each Janus particle in the direction it is orientated. The isolated propulsion speed in the absence of other particles, but in the presence of the chemical fuel, is v_0. In the most general case, this can be set individually for each particle and be time-dependent, but in the present simulations, we assume that it is constant and taken from our experimental observations of a Janus particle in infinite dilution (isolation). The second term represents the advection of the Janus particle by the fluid flow created by all of the other cells translating and is given explicitly in eq 5. The third term $\mathbf{F}$ is the short-range purely repulsive force modeled by a Yukawa potential (e.g., see Drescher et al.[37] or for similar results use a truncated Lennard−Jones potential[39]). This term is designed to repel all particles within one particle length to account for the excluded volume occupied by the Janus particle surrounding its center of mass. The fourth term in eq 6 represents translational diffusion and is modeled as a white noise process and is formally represented as the derivative of a Weiner process. The strength of the translational diffusion is given by D_t. The coefficient as defined in (6) represents the modified drag force exhibited on the translating Janus particle due to the effects of the boundary on the particles. By using these hinderance terms, we can simulate the three-dimensional thin-film domain with a two-dimensional model.

From the balance of torques on each particle, we arrive at eq 7 governing the dynamics of the orientation of the ith particle. The first term is derived from Jeffery's equations[40] and allows the point dipoles to interact with the fluid as if they were prolate ellipsoids. Only the contribution to orientation dynamics from the local vorticity remains for spherical particles. Traditionally, there is an additional term due to the rate of strain, but this term is proportional to the Bretherton constant, which is zero for spheres. The last term represents rotational diffusion and is also modeled as a white noise process with strength D_θ. The rotational hinderance capturing the orientation drag, q_θ, slows the angular velocity of each Janus particle as a function of the distance from the boundary.

The simulations were run with $N = 5$ particles mimicking a semidilute regime, but the model can account for any number. A computational domain of size $L \times L$, where $L = 75l$ is 75 times the size on an individual particle, was employed. The concentration can be measured as an effective area fraction $\rho = N\pi l^2/4L^2$, and simulation concentrations were chosen to match experimental densities. In addition, the simulations were performed with periodic boundary conditions to eliminate any finite size effects associated with the boundaries in the x

DOI: 10.1021/acsomega.9b00765
ACS Omega 2019, 4, 13034−13041

and y directions. Parameters used in the simulation can be found in Table 1 below.

Table 1. Simulation Conditions

simulation conditions	
particle radius (μm)	2.5
temperature (K)	298
fluid viscosity (Pa s)	0.00089
particle density (kg/m^3)	1055
initial particles in frame (#)	5
total number of frames for each video	500
time step (s)	0.06
total simulation time (s)	30
translation diffusion coefficient in bulk (m^2/s)	9.80998×10^{-14}
rotational diffusion coefficient in bulk (r^2/s)	0.01177198

3. METHODS

3.1. Fabricating Janus Particles. Molecular probe polystyrene sulfate latex beads with nominally 5 μm diameter were obtained from Fisher Scientific (Lot #1964358). The suspension of polystyrene spheres was washed with ultrapure water via ultrasonication and transferred to ethanol for suspension prior to monolayer fabrication. Spin coating was used to prepare a monolayer of the native polystyrene spheres on a 20 x 20 mm silicon wafer that was made hydrophilic using a plasma cleaner (PDC 32G). Approximately 15 μL of solution was dispersed onto each of the 20 x 20 mm silicon wafers positioned inside the spin coater. The suspension drop was spun down first for 20 s at 300 rpm and then for 40 s at 3000 rpm.

For the platinum deposition process, the silicon wafers were attached and secured onto prelabeled microscope slides using a high-temperature adhesive tape. The platinum vapor deposition on the 2D close-packed colloidal monolayer was performed inside a vacuum with an angle of incidence θ = 0° (the stationary substrate is positioned parallel to the ground and perpendicular to the platinum vapor). The chamber housing the e-beam evaporator was pumped to reach pressures below 10^{-5} Pa. Platinum was deposited to a nominal thickness of 20 nm at a rate of 0.25 Å/s. Finally, Janus particles were redispersed by first submerging the wafers in ultrapure water using a 50 mL centrifuge tube. The tubes were sonicated for at least 45 min to ensure maximum desorption of particles. The suspension containing the Janus particles was then centrifuged for ∼5 min at 4000 rpm, and the supernatant was removed. The process was repeated twice, and the finally collected volume was concentrated into a 1 mL suspension consisting of Janus particles and ultrapure water. Nominally 20 nm diameter sulfate-modified polystyrene particles obtained from Life Technologies (Lot #1677600) were utilized for some experiments. These nanoparticles had electrophoretic mobility of -3.65 ± 0.11 μm cm/(V s). The nanoparticle suspension was sonicated for 20 min followed by vortex-mixing at 4000 rpm for 2 min prior to addition to the sample contained in the fluid cell. Finally, poly(ethylene glycol) (PEG, Alfa Aesar, Lot #1019473) with a molecular weight MW = 6000 was used as received for the follow-up control experiments with uncharged depletants.

3.2. Preparation of Fluid Cell and Image Collection. The fluid cell was installed onto a prewashed and sonicated microscope slide using a Secure-Seal spacer (Lot #1870350) with a 9 mm diameter and a 0.12 mm depth and coverslip on top. The suspension of Janus particles was pipetted into the fluid cell with the appropriate amount of H_2O_2 for each experimental condition. Janus particle concentration was set at infinite dilution (<10 particles in ROI) near a boundary to minimize the effects of surface interactions that could arise between neighboring particles. The suspension containing Janus particles was first pipetted into the cell, followed by the addition of a specified volume of nanoparticle suspension. Finally, H_2O_2 was pipetted into the fluid cell and immediately closed with a coverslip to minimize evaporation.

Images were collected and analyzed at a frame rate of between 2.6 and 16.2 frames per second of an infinitely dilute suspension of particles settled near a boundary. A total of 81 videos at various conditions were obtained, with the majority containing >1000 frames or more and between 1 and 5 particles in the region of interest for the entire video. The standard deviation of multiple particles is reported herein as error bars. Image stacks were initially filtered in Fiji (https://fiji.sc/), particles were subsequently identified and tracked, and trajectories were calculated from an existing algorithm executed in MATLAB.[41,42] The MSD $\langle r^2 \rangle$ was calculated from these trajectories. In the absence of H_2O_2, the MSD curve was fit with a linear relationship (see eq 8), whereas in the presence of H_2O_2, the MSD was fit with the expression for a self-propelled particle at short times when compared to that at rotational diffusion time $1/D_r \sim 85$ s (see eq 9)[43]

$$\langle r^2 \rangle = 4D_0\tau \tag{8}$$

$$\langle r^2 \rangle = 4D_0\tau + v_p^2\tau^2 \tag{9}$$

All experimental data was fit for $\tau < 5$ s, which satisfies the short-time criteria for eq 9. Fits reported herein were from a single-parameter fit in each scenario. The fit parameter was D_0 in eq 8 for experiments not containing H_2O_2, while the fit parameter was v_s in eq 9 for experiments containing H_2O_2, with D_0 fixed at a value obtained from previous measurements. Note that in addition to the single-parameter fit in the latter case with H_2O_2, we also conducted a two-parameter fit for both D_0 and v_s. Differences in the value of v_s between the two fits were typically <10%.

4. RESULTS AND DISCUSSION

4.1. Propulsion of Janus Particles. The speed response of Janus particles with a platinum cap was measured as a function of H_2O_2 concentration. The apparent speed of the Janus particles increased roughly linearly with increasing peroxide concentration (see Figure 2). Note the large error bars associated with these data. The origin of error arises from multiple factors, including particle fabrication and the nature of the experiment itself. A platinum cap with 50% coverage, a Janus particle, will result when a monolayer of particles is situated on a substrate normal to the deposition direction. However, variations in cap thickness from particle to particle will arise during fabrication because of multilayer regions or other departures from a particle monolayer situated perpendicular to the deposition source. Further, slight variations in particle size, inherent to our particle sample, will alter the propulsion speed. The values of propulsion speed reported here are systematically lower than those reported elsewhere,[43] although that work utilized particles with significantly smaller radii than those used herein (∼1.6 vs

DOI: 10.1021/acsomega.9b00765
ACS Omega 2019, 4, 13034−13041

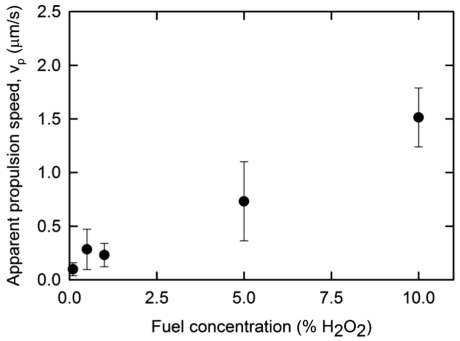

Figure 2. Apparent speed of Janus particles. The apparent speed of Janus particles increased linearly with increasing fuel concentration. We chose to focus experiments for the remainder of the article on a fuel concentration of 5% to not only drive sufficient deterministic motion but also mitigate deleterious effects of bubbles.

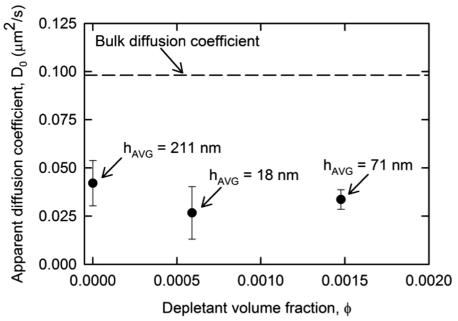

Figure 3. Apparent diffusion coefficient of Janus particles as a function of depletant concentration. The diffusion coefficient at a depletant volume fraction $\phi = 0$ was hindered because the particles settle to the bottom boundary under the influence of gravity. Following the addition of depletants, Janus particles moved closer to the boundary because of increased attractive interaction between the particle and wall. The decrease in average separation distance was nonmonotonic, which could result from structural forces that arise in suspensions of strongly charged nanoparticles.[47]

~2.5 μm). Previous work has reported an inverse dependence of propulsion speed on particle radius.[44] Another factor contributing to the error in these measurements is that deterministic motion from propulsion is superimposed on Brownian fluctuations that are random. The stochastic nature of these experiments produces some error intrinsic to the measurement.

Catalytic active Janus particles may produce macroscopic bubbles at some conditions. Bubble generation was significant at conditions where either the particle concentration or H_2O_2 concentration was large. A large particle concentration provided a large area for the catalytic activity to produce significant amounts of O_2 as product. Whereas a large H_2O_2 concentration provides a large concentration of reactant to produce a significant product. In either case, significant bubble production was detrimental to image capture. In response to these concerns, experiments described for the remainder of this article were conducted at conditions that balanced these two deleterious effects, large error as compared to speed and bubble generation. We chose to work at infinite dilution and 5% H_2O_2 concentration because these conditions resulted in active particles with a speed that was sufficiently large to track, yet did not produce large quantities of macroscopic bubbles detrimental to imaging.

4.2. Propulsion of Janus Particles in the Presence of Depletants. The addition of nonadsorbing nanoparticles will act as depletants in a suspension of colloidal particles.[45−47] Herein, negatively charged 20 nm particles were added to induce a conservative depletion attraction between the Janus particles and nearby boundary. Initial experiments measured the lateral diffusion coefficient for Janus particles in the presence of depletants, but the absence of H_2O_2. The volume fractions of nanoparticles were $\phi = 0$, 0.00059, and 0.0015. Note that even in the absence of depletants, the diffusion coefficient was strongly hindered by the nearby boundary (see Figure 3). The addition of depletants further decreased the diffusion coefficient as a consequence of an attractive depletion interaction between the Janus particle and boundary (see Figure 3). The average separation distance h_{AVG} was inferred from the relationship between the diffusion coefficient and separation distance (see eqs 1 and 2). These data show that the average separation distance decreased from h_{AVG} = 211 nm at $\phi = 0$ to h_{AVG} < 100 nm upon the addition of depletants ϕ = 0.00059 and ϕ = 0.0015. Note also a small increase in average height at larger volume fractions. A reduction in the attractive depletion force may occur at larger volume fractions as a consequence of oscillatory or structural forces found in charged systems.[47]

Next, experiments were conducted to track the propulsion of Janus particles in the presence of nanoparticles and in 5% H_2O_2. The impact of adding nanoparticles was immediately clear. The MSD from Janus particles suspended in 5% H_2O_2 and nanoparticles was smaller in magnitude and revealed a linear dependence on lag time $\sim\tau$. This departs from the nonlinear dependence on lag time $\sim\tau^2$ observed for experiments with Janus particles in the presence of H_2O_2 and absence of nanoparticles. Figure 4 shows a typical mean-squared displacement for a Janus particle in 5% H_2O_2 in the presence and absence of depletants.

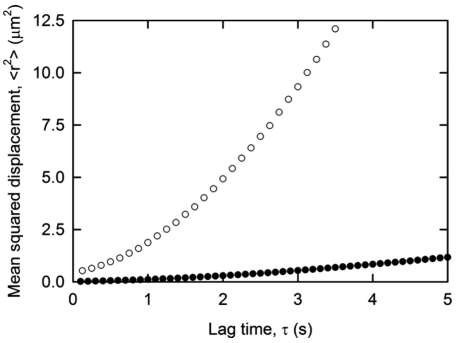

Figure 4. Mean-squared displacement (MSD) of a Janus particle in 5% H_2O_2 in the absence (open circles) and presence (black filled circles) of 20 nm nanoparticles. The MSD of a Janus particle in the absence of 20 nm particles depended on the square of lag time, while the MSD depended linearly on lag time following the addition of the nanoparticles. The τ^2 dependence indicated propulsion (see eq 8), while the τ indicated a purely Brownian motion (see eq 9).

The relationship between MSD and lag time transitioned from one characteristic of an active particle (see eq 9) to one characteristic of a purely Brownian particle (see eq 8). Apparent propulsion speed was calculated from these experiments. As gleaned from the MSD curves, the addition of nanoparticles strongly quenched the propulsion speed to near 0 μm/s (see Figure 5). The decrease in propulsion speed

DOI: 10.1021/acsomega.9b00765
ACS Omega 2019, 4, 13034−13041

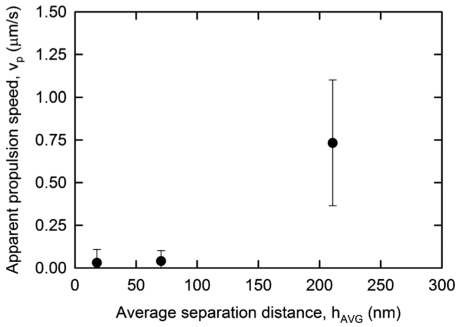

Figure 5. Apparent propulsion speed was strongly quenched following the addition of depletants. Propulsion speed decreased with a decrease in the average separation distance of the Janus particle in response to the presence of 20 nm nanoparticles.

correlated with a decrease in the average separation distance. Of particular interest was that the apparent propulsion speed decreased monotonically with an average separation distance, but not depletant volume fraction. These data corroborate the potential importance of structural forces at high depletant volume fraction, as first shown in Figure 3.

4.3. Role of Nanoparticles in Quenching Janus Particle Propulsion. Simulations were developed to calculate the expected reduction in propulsion speed because of the change in average separation distance. Initially, agent-based simulations were conducted to determine the appropriate free propulsion speed of a dipolar Janus particle at infinity in the absence of all other particles. This set of calibration simulations was conducted such that the free propulsion speed was set and the apparent propulsion speed of particles at an average separation distance of ∼200 nm was measured. The apparent propulsion speed scaled linearly with the free propulsion speed (see Figure 6). This set of calibration data was necessary

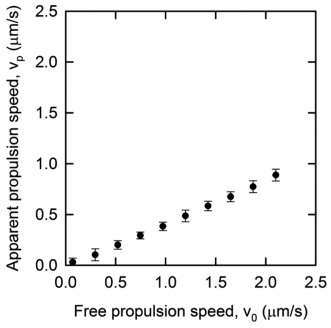

Figure 6. Apparent propulsion speed v_p as a function of the free propulsion speed v_0 for a Janus particle at h_{AVG} ∼ 200 nm. The apparent propulsion speed scaled as roughly half that of the free propulsion speed. The free propulsion speed was calibrated with this data such that v_0 = 1.38 μm/s for the remainder of the experiments described herein.

because the apparent propulsion speed of a Janus particle, measurable in the experiment, includes many factors such as hydrodynamic advection, self-propulsion, and diffusion. However, in the model, it is critical to set the isolated free propulsion speed, which does not depend on the effect of other particles or diffusion. Thus, we estimated the free propulsion speed by generating a simulation fixing all parameters to the values in Table 1 and varying until the apparent net propulsion speed matches the experimental observation at 200 nm. From this point on, it will be that constant in all subsequent simulations. We also note that the free propulsion speed is typically larger than the apparent speed due to the fact that diffusion and the hydrodynamic hindrances lead to decreases in the observed rate of motion.

Once the necessary free speed was determined = 1.38 μm/s, a series of simulations were conducted at systematically different heights to calculate the impact of h_{AVG} on the apparent propulsion speed. Note that simulations were conducted in a quasi-2D layer with all particles at a fixed separation distance. Constructing the simulations in this fashion isolated the impact of hydrodynamics. Apparent propulsion speed decreased monotonically with decreased average separation distance (see Figure 7).

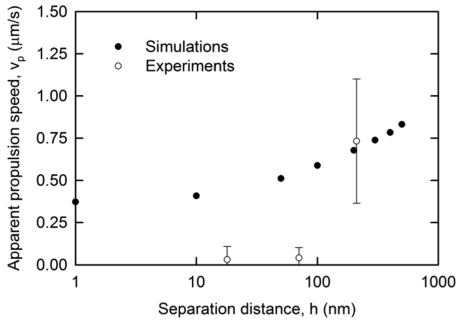

Figure 7. Apparent propulsion speed as a function of separation distance from simulation and experiment. Apparent propulsion speed in experiments was strongly quenched following the addition of nanoparticles. However, there was only a minor reduction in propulsion speed in comparison to experimental observations. These data suggest that the reduction in propulsion speed cannot solely be attributed to the hydrodynamic hindrance of the form used herein.

Data summarized in Figure 7 provide a partial explanation for experimental observations. In simulations, the propulsion speed at h_{AVG} < 100 nm was reduced by ∼1/3 of the value at h_{AVG} ∼ 200 nm. However, experimental observations indicated that the propulsion was reduced to nearly 0 μm/s. The additional reduction observed in experiments could be a consequence of a number of contributing factors. One such additional mechanism is in the change in fluid conductivity as a consequence of adding charged nanoparticles. The conductivity of the depletant suspension was measured to be 2.34, 18.5, and 36.45 μS/cm for ϕ = 0, 0.00059, and 0.0015, respectively. These values correspond to resistivity values between 4274 and 274 Ω m. Such changes in conductivity have been reported to reduce the catalytic propulsion speed by an order of magnitude.[28]

We conducted control experiments to separate the impact of fluid conductivity and depletant concentration. Digital video microscopy of a new batch of Janus particles prepared as described above was conducted in (i) 5% H_2O_2, (ii) 5% H_2O_2 with a systematically adjusted concentration of PEG, and (iii) 5% H_2O_2 with a systematically adjusted concentration of NaCl. PEG had a negligible impact on solution conductivity, with the highest PEG concentration (ϕ = 0.006) having a fluid conductivity < 10 μS/cm. We also systematically adjusted concentrations of NaCl between 0.075 and 0.6 mM such that the solution conductivity ranged from ultrapure water up to 79.57 μS/cm, which matched and went beyond our previously described experiments with charged nanoparticles. Figure 8

DOI: 10.1021/acsomega.9b00765
ACS Omega 2019, 4, 13034−13041

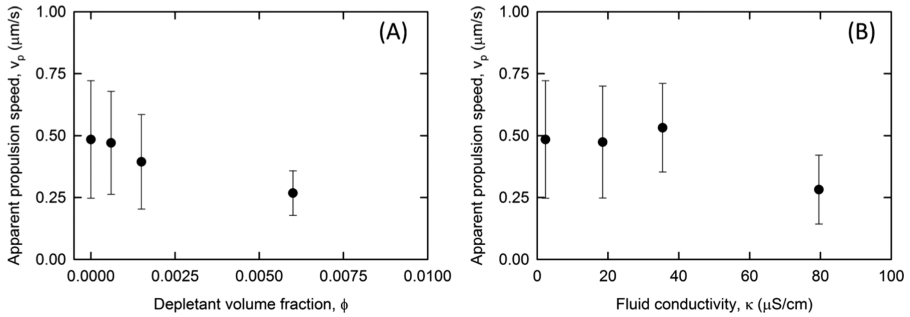

Figure 8. Apparent propulsion speed for Janus particles in uncharged depletant poly(ethylene glycol) (PEG) and NaCl. (A) Apparent propulsion speed decreased as uncharged depletant volume fraction increased. PEG suspensions had negligible changes in conductivity, yet still impacted the swim speed. Similarly, (B) the apparent propulsion speed decreased at larger electrolyte conductivity, which was adjusted by changing the NaCl concentration between 0.075 and 0.6 mM. Error bars are the standard deviation calculated from multiple particles (N_p) in multiple fluid cells. The number of particles N_p as a function of increasing depletant concentration were N_p = 29, 13, 14, and 15 and as a function of increasing conductivity N_p = 29, 14, 15, and 9.

shows the change in apparent swim speed as a function of PEG volume fraction (see Figure 8A) and solution conductivity adjusted via the addition of NaCl (see Figure 8B). These experiments revealed that both uncharged depletants and increases in solution conductivity will quench the propulsion of catalytic active particles. These control experiments, together with our earlier described measurements with charged nanoparticles as depletant, suggest that such effects can be synergized in the case when both are present.

Although measurements with charged depletants, uncharged depletants, and salt demonstrate that depletion and solution conductivity have a synergistic effect on the propulsion of active Janus particles, there are additional potential mechanisms for propulsion reduction. The dynamic drag associated with the nanoparticles surrounding the Janus particle could also reduce swimming. A colloidal particle will be enveloped by some equilibrium distribution of nanoparticles. When moving, however, the Janus particle will need to move this cloud of nanoparticles, thereby creating additional hindrance that may slow the propulsion. Finally, when the Janus particle is almost touching the boundary, nonlinear lubrication forces between the particle and the boundary may become a dominant interaction, which is not explicitly accounted for in the hydrodynamic models (6) and (7).

5. CONCLUSIONS

Experiments and simulations were conducted to elucidate the impact of charged nanoparticles on the propulsion of active Janus particles. Digital video microscopy measurements in conjunction with particle tracking revealed that Janus particles propel in the presence of H_2O_2, but quench to nearly nil speed in the presence of nanoparticles. Further, experiments revealed that the reduction of the average separation distance of passive particles was nonmonotonic with nanoparticle volume fraction, suggesting that structural forces will play a role at high volume fractions. Agent-based simulations were conducted of dipolar Janus particles at systematically varied separation distance to determine the influence of hydrodynamic quenching of propulsion. The speed of Janus particles decreased when the separation distance was systematically decreased. Although the trend from simulations qualitatively matched results from experiments, the magnitude of quenching determined from simulations was smaller than what was found in experiments. Simulation results suggest some influence of hydrodynamic quenching when bringing an active colloid closer to a nearby boundary. In addition, the increase in fluid conductivity associated with the addition of nanoparticles is a factor for the difference between experiments and simulated propulsion speeds. Follow-up experiments delineating the impact of depletion and conductivity showed that both likely contribute to the reduction of speed for an active Janus particle. These data show the synergistic effects arising from depletion, and changes in conductivity should be considered when studying the dynamics of active Janus particles near a boundary.

AUTHOR INFORMATION

Corresponding Author

*E-mail: c.wirth@csuohio.edu, christopher.wirth@case.edu.

ORCID

Christopher L. Wirth: 0000-0003-3380-2029

Author Contributions

§M.W.I. and N.R.B. contributed equally to this work.

Author Contributions

The manuscript was written through contributions of all authors. All authors have given approval to the final version of the manuscript. M.W.I., M.A.K., and C.L.W. conducted the experiments and analyzed the results. N.R.B. and S.D.R. developed the mathematical model, conducted simulations, and analyzed the results.

Notes

The authors declare no competing financial interest.

ACKNOWLEDGMENTS

This work was supported by the Cleveland State University Office of Research Startup Fund, the National Science Foundation CAREER Award, NSF no. 1752051, and an Undergraduate Summer Research Award (M.W.I.).

REFERENCES

(1) Baraban, L.; Tasinkevych, M.; Popescu, M. N.; Sanchez, S.; Dietrich, S.; Schmidt, O. G. Transport of cargo by catalytic Janus micro-motors. *Soft Matter* **2012**, *8*, 48−52.

(2) Ma, X.; Hahn, K.; Sanchez, S. Catalytic Mesoporous Janus Nanomotors for Active Cargo Delivery. *J. Am. Chem. Soc.* **2015**, *137*, 4976−4979.

(3) Vicsek, T.; Czirók, A.; Ben-Jacob, E.; Cohen, I.; Shochet, O. Novel Type of Phase Transition in a System of Self-Driven Particles. *Phys. Rev. Lett.* **1995**, *75*, 1226−1229.

DOI: 10.1021/acsomega.9b00765
ACS Omega 2019, 4, 13034−13041

(4) Toner, J.; Tu, Y. Long-Range Order in a Two-Dimensional Dynamical *XY* Model: How Birds Fly Together. *Phys. Rev. Lett.* **1995**, *75*, 4326−4329.
(5) Sundararajan, S.; Lammert, P. E.; Zudans, A. W.; Crespi, V. H.; Sen, A. Catalytic motors for transport of colloidal cargo. *Nano Lett.* **2008**, *8*, 1271−1276.
(6) Kagan, D.; Calvo-Marzal, P.; Balasubramanian, S.; Sattayasamitsathit, S.; Manesh, K. M.; Flechsig, G.-U.; Wang, J. Chemical Sensing Based on Catalytic Nanomotors: Motion-Based Detection of Trace Silver. *J. Am. Chem. Soc.* **2009**, *131*, 12082−12083.
(7) Wu, J.; Balasubramanian, S.; Kagan, D.; Manesh, K. M.; Campuzano, S.; Wang, J. Motion-based DNA detection using catalytic nanomotors. *Nat. Commun.* **2010**, *1*, No. 36.
(8) Ebbens, S. J. Active colloids: Progress and challenges towards realising autonomous applications. *Curr. Opin. Colloid Interface Sci.* **2015**, *21*, 14−23.
(9) Wang, W.; Duan, W.; Ahmed, S.; Mallouk, T. E.; Sen, A. Small power: Autonomous nano- and micromotors propelled by self-generated gradients. *Nano Today* **2013**, *8*, 531−534.
(10) Buttinoni, I.; Bialké, J.; Kümmel, F.; Löwen, H.; Bechinger, C.; Speck, T. Dynamical Clustering and Phase Separation in Suspensions of Self-Propelled Colloidal Particles. *Phys. Rev. Lett.* **2013**, *110*, No. 238301.
(11) Ma, F.; Wang, S.; Wu, D. T.; Wu, N. Electric-field−induced assembly and propulsion of chiral colloidal clusters. *Proc. Natl. Acad. Sci. U.S.A.* **2015**, *112*, 6307−6312.
(12) Paxton, W. F.; Kistler, K. C.; Olmeda, C. C.; Sen, A.; St. Angelo, S. K.; Cao, Y.; Mallouk, T. E.; Lammert, P. E.; Crespi, V. H. Catalytic Nanomotors: Autonomous Movement of Striped Nanorods. *J. Am. Chem. Soc.* **2004**, *126*, 13424−13431.
(13) Du, D.; Hilou, E.; Biswal, S. L. Reconfigurable paramagnetic microswimmers: Brownian motion affects non-reciprocal actuation. *Soft Matter* **2018**, *14*, 3463−3470.
(14) Jalilvand, Z.; Pawar, A. B.; Kretzschmar, I. Experimental Study of the Motion of Patchy Particle Swimmers Near a Wall. *Langmuir* **2018**, *34*, 15593−15599.
(15) Rashidi, A.; Issa, M. W.; Martin, I. T.; Avishai, A.; Razavi, S.; Wirth, C. L. Local Measurement of Janus Particle Cap Thickness. *ACS Appl. Mater. Interfaces* **2018**, *10*, 30925−30929.
(16) Pawar, A. B.; Kretzschmar, I. Fabrication, assembly, and application of patchy particles. *Macromol. Rapid Commun.* **2010**, *31*, 150−168.
(17) Pawar, A. B.; Kretzschmar, I. Multifunctional patchy particles by glancing angle deposition. *Langmuir* **2009**, *25*, 9057−9063.
(18) He, Z.; Kretzschmar, I. Template-assisted GLAD: approach to single and multipatch patchy particles with controlled patch shape. *Langmuir* **2013**, *29*, 15755−15761.
(19) Ebbens, S.; Tu, M.-H.; Howse, J. R.; Golestanian, R. Size dependence of the propulsion velocity for catalytic Janus-sphere swimmers. *Phys. Rev. E* **2012**, *85*, No. 020401.
(20) Popescu, M. N.; Uspal, W. E.; Domínguez, A.; Dietrich, S. Effective Interactions between Chemically Active Colloids and Interfaces. *Acc. Chem. Res.* **2018**, *51*, 2991−2997.
(21) Anekal, S. G.; Bevan, M. A. Interpretation of conservative forces from Stokesian dynamic simulations of interfacial and confined colloids. *J. Chem. Phys.* **2005**, *122*, No. 034903.
(22) Simmchen, J.; Katuri, J.; Uspal, W. E.; Popescu, M. N.; Tasinkevych, M.; Sánchez, S. Topographical pathways guide chemical microswimmers. *Nat. Commun.* **2016**, *7*, No. 10598.
(23) Spagnolie, S. E.; Lauga, E. Hydrodynamics of self-propulsion near a boundary: predictions and accuracy of far-field approximations. *J. Fluid Mech.* **2012**, *700*, 105−147.
(24) Mozaffari, A.; Sharifi-Mood, N.; Koplik, J.; Maldarelli, C. Self-diffusiophoretic colloidal propulsion near a solid boundary. *Phys. Fluids* **2016**, *28*, No. 053107.
(25) Uspal, W. E.; Popescu, M. N.; Dietrich, S.; Tasinkevych, M. Self-propulsion of a catalytically active particle near a planar wall: from reflection to sliding and hovering. *Soft Matter* **2015**, *11*, 434−438.
(26) Yang, F.; Mou, F.; Jiang, Y.; Luo, M.; Xu, L.; Ma, H.; Guan, J. Flexible Guidance of Microengines by Dynamic Topographical Pathways in Ferrofluids. *ACS Nano* **2018**, *12*, 6668−6676.
(27) Das, S.; Garg, A.; Campbell, A. I.; Howse, J.; Sen, A.; Velegol, D.; Golestanian, R.; Ebbens, S. J. Boundaries can steer active Janus spheres. *Nat. Commun.* **2015**, *6*, No. 8999.
(28) Brown, A.; Poon, W. Ionic effects in self-propelled Pt-coated Janus swimmers. *Soft Matter* **2014**, *10*, 4016−4027.
(29) Rashidi, A.; Wirth, C. L. Motion of a Janus particle very near a wall. *J. Chem. Phys.* **2017**, *147*, No. 224906.
(30) Ryan, S. D.; Haines, B. M.; Berlyand, L.; Ziebert, F.; Aranson, I. S. Viscosity of bacterial suspensions: Hydrodynamic interactions and self-induced noise. *Phys. Rev. E* **2011**, *83*, No. 050904.
(31) Ryan, S. D.; Sokolov, A.; Berlyand, L.; Aranson, I. S. Correlation properties of collective motion in bacterial suspensions. *New J. Phys.* **2013**, *15*, No. 105021.
(32) Ariel, G.; Sidortsov, M.; Ryan, S. D.; Heidenreich, S.; Bär, M.; Be'er, A. Collective dynamics of two-dimensional swimming bacteria: Experiments and models. *Phys. Rev. E* **2018**, *98*, No. 032415.
(33) Sokolov, A.; Aranson, I. S.; Kessler, J. O.; Goldstein, R. E. Concentration Dependence of the Collective Dynamics of Swimming Bacteria. *Phys. Rev. Lett.* **2007**, *98*, No. 158102.
(34) Lushi, E.; Wioland, H.; Goldstein, R. E. Fluid flows created by swimming bacteria drive self-organization in confined suspensions. *Proc. Natl. Acad. Sci. U.S.A.* **2014**, *111*, 9733−9738.
(35) Saintillan, D.; Shelley, M. J. Instabilities, pattern formation, and mixing in active suspensions. *Phys. Fluids* **2008**, *20*, No. 123304.
(36) Hernandez-Ortiz, J. P.; Stoltz, C. G.; Graham, M. D. Transport and Collective Dynamics in Suspensions of Confined Swimming Particles. *Phys. Rev. Lett.* **2005**, *95*, No. 204501.
(37) Drescher, K.; Dunkel, J.; Cisneros, L. H.; Ganguly, S.; Goldstein, R. E. Fluid dynamics and noise in bacterial cell−cell and cell-surface scattering. *Proc. Natl. Acad. Sci. U.S.A.* **2011**, *108*, 10940−10945.
(38) Cui, B.; Diamant, H.; Lin, B.; Rice, S. A. Anomalous Hydrodynamic Interaction in a Quasi-Two-Dimensional Suspension. *Phys. Rev. Lett.* **2004**, *92*, No. 258301.
(39) Ryan, S. D.; Ariel, G.; Be'er, A. Anomalous Fluctuations in the Orientation and Velocity of Swarming Bacteria. *Biophys. J.* **2016**, *111*, 247−255.
(40) Jeffery, G. B. The Motion of Ellipsoidal Particles Immersed in a Viscous Fluid. *Proc. R. Soc. A* **1922**, *102*, 161−179.
(41) Furst, E. M. *Particle Tracking with Matlab*, 2015.
(42) Crocker, J.; Grier, D.; Crocker, J.; Grier, D. Methods of Digital Video Microscopy for Colloidal Studies. *J. Colloid Interface Sci.* **1996**, *179*, 298−310.
(43) Howse, J. R.; Jones, R. A. L.; Ryan, A. J.; Gough, T.; Vafabakhsh, R.; Golestanian, R. Self-Motile Colloidal Particles: From Directed Propulsion to Random Walk. *Phys. Rev. Lett.* **2007**, *99*, 8−11.
(44) Ebbens, S.; Tu, M. H.; Howse, J. R.; Golestanian, R. Size dependence of the propulsion velocity for catalytic Janus-sphere swimmers. *Phys. Rev. E* **2012**, *85*, 1−4.
(45) Sharma, A.; Walz, J. Y. Direct measurement of the depletion interaction in a charged colloidal dispersion. *J. Chem. Soc., Faraday Trans.* **1996**, *92*, 4997−5004.
(46) Sober, D. L.; Walz, J. Y. Measurement of Long Range Depletion Energies between a Colloidal Particle and a Flat Surface in Micellar Solutions. *Langmuir* **1995**, 2352−2356.
(47) Piech, M.; Walz, J. Y. Direct Measurement of Depletion and Structural Forces in Polydisperse, Charged Systems. *J. Colloid Interface Sci.* **2002**, *253*, 117−129.

DOI: 10.1021/acsomega.9b00765
ACS Omega 2019, 4, 13034−13041